Applied Physics Express **5** (2012) 103002
http://dx.doi.org/**10.1143/APEX.5.103002**

Stress-Induced Perpendicular Magnetization in Epitaxial Iron Garnet Thin Films

Masashi Kubota[1,2*], Atsushi Tsukazaki[3,4], Fumitaka Kagawa[3,5], Keisuke Shibuya[1†], Yusuke Tokunaga[1], Masashi Kawasaki[1,3], and Yoshinori Tokura[1,3]

[1]*Correlated Electron Research Group (CERG) and Cross-Correlated Materials Research Group (CMRG), RIKEN Advanced Science Institute, Wako, Saitama 351-0198, Japan*
[2]*Advanced Compound Semiconductors R&D Center, ROHM Co., Ltd., Kyoto 615-8585, Japan*
[3]*Department of Applied Physics and Quantum Phase Electronics Center (QPEC), University of Tokyo, Bunkyo, Tokyo 113-8656, Japan*
[4]*PRESTO, Japan Science and Technology Agency, Bunkyo, Tokyo 113-8656, Japan*
[5]*CREST, Japan Science and Technology Agency, Bunkyo, Tokyo 113-8656, Japan*

Received August 9, 2012; accepted August 29, 2012; published online September 13, 2012

We have grown pseudomorphic $Tm_3Fe_5O_{12}$ films (46–350 nm in thickness) with perpendicular magnetization on (111) $Gd_3Ga_5O_{12}$ substrates. Among various garnets, $Tm_3Fe_5O_{12}$ is selected because of a negatively large magnetostriction constant to overcome strong shape anisotropy in very thin films. A stress-induced anisotropy field as large as +25 kOe is estimated by calculation under a moderate in-plane tensile strain of +0.49%. The magnetization hysteresis loop and magnetic domain structure indicate the perpendicular easy axis. The domain size (W) in its maze pattern varies from 500 to 960 nm with increasing thickness (t) and agrees well with a scaling law of $W \propto \sqrt{t}$.

Iron garnets, $RE_3Fe_5O_{12}$ (RE: rare earth), are one of the most extensively studied insulating soft magnets.[1)] Decades ago, the motivation was to apply them to such devices as magnetic bubble memories[2)] and magneto-optics.[3)] Recently, iron garnets have attracted revived interest for microwave devices,[4)] multiferroics in superlattices,[5)] and possible electric field control of domain wall motion.[6)] If small magnetic bubbles could be manipulated by an electric field, one may be able to realize low-energy-dissipation magnetic memories. For these devices with a thin film form, magnetic anisotropy has to be tuned so as to show the perpendicular easy axis, by overcoming the shape anisotropy. When films were thick (>1 μm), it was not so difficult to fulfil this requirement with the use of stress-induced anisotropy originating predominantly from the thermal expansion mismatch between substrate and film as demonstrated for a chemical vapor deposition technique.[7)] More recently, growth-induced anisotropy has been employed in the case of a liquid phase epitaxy (LPE) technique, realizing the most reliable manufacturing method for practical devices.[8)] Since the magnetic domain width W scales with the film thickness t as $W \propto \sqrt{t}$ (p. 138 of ref. 1), one needs to grow thinner films to realize a smaller domain size.

Recently, pulsed laser deposition (PLD) has been applied to garnet thin films to fabricate relatively thin (<1 μm) films and heterostructures.[4,5,9–12)] The thickness controllability in PLD surpasses that of LPE. With a high repetition of ablation lasers,[10)] one can readily grow thin films with magnetic properties similar to those of bulk crystals.[11)] However, perpendicular magnetization has not been confirmed for thin (<100 nm) epitaxial films.[4,9–12)] Our approach in this study is to use a stress-induced anisotropy field to overcome the strong shape anisotropy, because PLD is known to be useful for growing coherently strained pseudomorphic films. Since the crystallographic easy axis is ⟨111⟩ in garnet, we take (111)-oriented thin films as a possibly easier choice. In a material with negative (positive) magnetostriction constants λ_{111} (p. 75 in ref. 1), the magnetic easy axis tends to lie perpendicular to the thin-film plane under tensile (compressive) epitaxial strain. Effective anisotropy field (H_A) for (111) plane garnets can be derived by[7)]

$$H_A = \frac{-4K_1 - 9\lambda_{111}\sigma_{\parallel}}{3M}. \quad (1)$$

Here, K_1, $\sigma_{\parallel}$, and M are the first-order cubic anisotropy constant (p. 66 of ref. 1), in-plane stress, and spontaneous magnetization (p. 14 of ref. 1), respectively. The value of $\sigma_{\parallel}$ can be calculated by taking into account the elastic deformation tensor as[13)]

$$\sigma_{\parallel} = 6C_{44}\frac{C_{11}+2C_{12}}{C_{11}+2C_{12}+4C_{44}}\varepsilon_{\parallel}, \quad (2)$$

where C_{ij} and $\varepsilon_{\parallel}$ are the elastic stiffness constants and in-plane strain, respectively. We plot these values in Fig. 1 for various $RE_3Fe_5O_{12}$ calculated by assuming a coherently strained pseudomorphic structure on the most commonly used $Gd_3Ga_5O_{12}$ (GGG) substrate. Among the iron garnets, those having compensation temperatures near room temperature are not suitable for our purpose (shown by open symbols), because of smaller M. Also unsuitable are those locating outside of the hatched region in Fig. 1(b) having a larger lattice mismatch than 0.5% to the GGG substrate, because it will be difficult to maintain a pseudomorphic structure. From this consideration, the $Tm_3Fe_5O_{12}$ film on the GGG substrate appears to be the most plausible candidate; an H_A as large as +25 kOe is estimated for rather small in-plane strain (+0.49%) and stress (+1.4 GPa). Since the H_A is larger than the saturation field (H_s) of about 2 kOe under a perpendicular magnetic field for a typical stress-free garnet film with in-plane easy axis, it will be possible to overcome the shape anisotropy.[14)]

In this letter, we present the magnetic properties and domain structures of $Tm_3Fe_5O_{12}$ films with thicknesses ranging from 46 to 350 nm. The films are fully strained to exhibit a magnetization hysteresis that evidences the perpendicular easy axis. Magnetic force microscopy (MFM) images indicate a maze pattern typical for a perpendicularly magnetized film. The domain width ranges from approximately 500 to 960 nm in excellent accordance with a scaling law.

Epitaxial thin films of $Tm_3Fe_5O_{12}$ were grown on the (111) plane of GGG substrates (Saint-Gobain) by a PLD

*E-mail address: Masashi.Kubota@dsn.rohm.co.jp
†Present address: Correlated Electronics Group, National Institute of Advanced Industrial Science and Technology (AIST), Tsukuba, Ibaraki 305-8562, Japan.

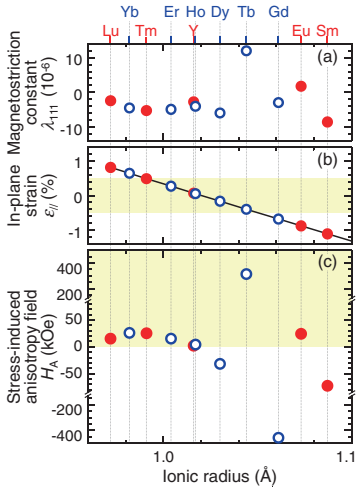

Fig. 1. Several magnetomechanical quantities for $RE_3Fe_5O_{12}$: Expected values of effective anisotropy field (H_A) in (c) are calculated from literature values of magnetostriction constants λ_{111} (p. 75 of ref. 1) shown in (a) and other parameters for $RE_3Fe_5O_{12}$ deduced using eqs. (1) and (2) for (111)-oriented films on $Gd_3Ga_5O_{12}$ substrate. The data are plotted as a function of ionic radius of RE^{3+}. In-plane strain $\varepsilon_{\parallel}$ is plotted in (b) assuming pseudomorphic structure. Among the garnets, those with and without compensation temperatures are shown with open and closed symbols, respectively.

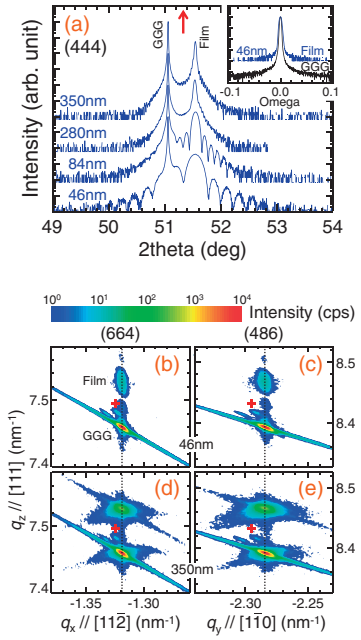

Fig. 2. (a) 2θ–ω XRD patterns for $Tm_3Fe_5O_{12}$ films grown on (111) GGG substrates. The film thickness was determined from Laue fringes near the (444) peak. The arrow indicates the peak position of bulk $Tm_3Fe_5O_{12}$ (p. 10 of ref. 1). The inset shows rocking curves measured at the (444) peak for the thinnest 46 nm film and GGG substrate. Reciprocal space mappings of the 46 (upper) and 350 nm (lower) films are shown for the (664) peaks (b, d) and for the (486) peaks (c, e), respectively. These films have a fully strained pseudomorphic structure as indicated by identical peak positions along in-plane directions (broken lines). Crosses indicate the peak positions for bulk $Tm_3Fe_5O_{12}$.

technique with a stoichiometric ceramics target. Focused KrF excimer laser pulses were impinged to the target placed 40 mm away from the substrate at a frequency of 80 Hz with a fluence of 0.6 J/cm^2. Films were grown at 800 °C in an oxygen atmosphere of 0.8 Torr. The growth rate was approximately 0.002 nm/pulse (0.16 nm/s). The crystalline structure was examined by high-resolution X-ray diffraction (XRD) both for symmetric diffraction and for reciprocal space mapping (RSM). The film thickness was evaluated from Laue fringes appearing near the (444) peak in the XRD pattern. The magnetic hysteresis loop was measured using a magnetic property measurement system (MPMS) equipped with a vibrating sample magnetometer (VSM) and a superconducting quantum interference device. The magnetic domain structure was revealed by noncontact-mode MFM measurement (Attocube SPMxs in PPMS).

Figure 2(a) displays the XRD patterns of four films having different film thicknesses. The peaks assignable to (444) diffraction are clearly observed. The rocking curve shown in the inset has a full width at half maximum as small as 18 arcsec for (444) diffraction, which is close to the values of the GGG substrate and the instrumental resolution. The RSM data around the (664) diffraction are shown in Figs. 2(b) and 2(d) for films with thicknesses of 46 and 350 nm, respectively. As indicated by dotted lines, the films have a pseudomorphic structure with the in-plane lattice constant identical to that of the substrate along the $\langle 11\bar{2}\rangle$ direction. The pseudomorphic structure along the $\langle 1\bar{1}0\rangle$ direction was also confirmed from RSM data for the (486) diffraction as shown in Figs. 2(c) and 2(e). The experimentally obtained in-plain strain is +0.49%, fairly agreeing with our assumption (+0.49%) taken for calculating the H_A shown in Fig. 1.

From the magnetization measurements, all the films shown in Fig. 3 are confirmed to have a perpendicular easy axis. Representative data for the thinnest sample (46 nm) are shown in Fig. 3(a). Both H_s and coercive fields are considerably smaller for the hysteresis loop under the out-of-plane field than that taken under the in-plane field. Although the thicker films also show the perpendicular magnetization, the values of H_s under the out-of-plane field and magnetization ratio ($M_{\parallel}/M_{\perp}$) defined as in-plane over out-of-plane components of magnetization at H_s increased with increasing film thickness from 145 Oe and 0.47 at 46 nm to 850 Oe and 0.78 at 350 nm (data not shown). This tendency may be due to the reduction of effective in-plane stress in the film. The broadening of reflection spots in RSM data were found for thicker samples even though the films maintain the pseudomorphic structure as shown in Figs. 2(d) and 2(e). A similar observation was reported for $Sm_3Fe_5O_{12}$ films on (100) GGG substrates.[15)]

Figures 3(b)–3(g) display a series of MFM images for the thinnest sample (46 nm) taken under various external magnetic fields applied in the perpendicular direction. Before the measurement, the film was demagnetized using a commercial demagnetizer for a cathode-ray display. Starting from (b) at the demagnetized state, the film was fully magnetized with a positive field of 200 Oe, and then the image was taken at 100 Oe (c). In the following, domain structures were observed with applying smaller negative fields (d–f) than the saturation field (−150 Oe). After applying a negatively larger field than the saturation one, the image was taken at zero field (g). Figure 3(b) shows a clear maze pattern composed of black and white contrast,[16)] where the domain width is around 500 nm and the black and white areas are nearly the same. The contrast pattern agrees with that expected for the perpendicular magnetization film, because

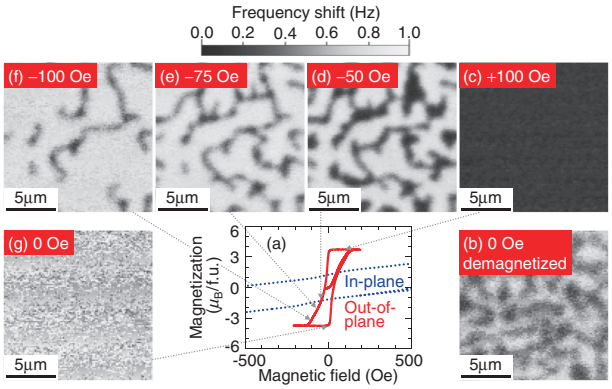

Fig. 3. (a) Magnetic field dependence of magnetization for the 46-nm-thick $Tm_3Fe_5O_{12}$ film. The hysteresis loops are taken at $T = 300$ K with the magnetic field applied along out-of-plane (solid line) and in-plane (broken line) directions. A series of magnetic force microscopy images are shown from (b) to (g) under various external magnetic fields in the perpendicular direction.

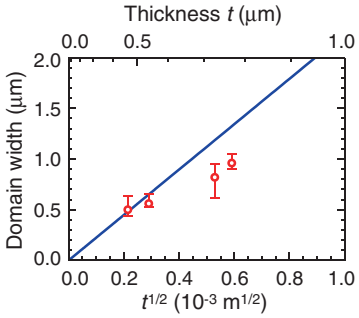

Fig. 4. Plots of domain width as a function of $\sqrt{t}$ (t: film thickness) for $Tm_3Fe_5O_{12}$ films on GGG substrates (circles). The corresponding t is shown in the upper horizontal axis. The solid line indicates the calculated relation according to eq. (3) for $Tm_3Fe_5O_{12}$ on GGG.

MFM measurement detects the magnetic field sourcing from the surface. If the film had an easy axis within the film plane, a closure magnetic domain structure, for example, would have dominated, resulting in the MFM image having two kinds of bands with significantly different sizes, one of which comes from magnetic domains irrespective of the magnetization direction and the other from narrow magnetic domain walls.[17] Therefore, the MFM image shown in Fig. 3(b) is a firm evidence of the perpendicular magnetization of the film. Figure 3(c) shows a single domain state. With applying a negative field, the areas with opposite magnetization (white region) are nucleated (d), and their area grows with applying higher negative fields as shown in Figs. 3(e) and 3(f). After completion of magnetization reversal, no domain feature is discerned even at zero field [Fig. 3(g)]. Very similar domain structures are confirmed for thicker films, which show slightly larger domain sizes.

In our films, the mean domain width W ranges from 500 to 960 nm, with increasing film thickness t from 46 to 350 nm. The W values estimated from MFM images are plotted in Fig. 4 as a function of $\sqrt{t}$. The magnetic domain width is known to depend on the thickness of the film t as

$$W = 2.72\sqrt{\frac{\sigma_w t}{4\pi M^2}}, \tag{3}$$

$$\sigma_w = 4\sqrt{AK_u}, \tag{4}$$

where σ_w, A, and K_u are the domain wall energy, exchange stiffness, and uniaxial anisotropy constant, respectively (p. 138 of ref. 1). Here, A for the substituted garnet is dependent on temperature T as[18]

$$A(T, T_N) = A_{YIG}(T) \times \frac{T_N - T}{T_{N,YIG} - T}, \tag{5}$$

where A_{YIG} is the exchange stiffness for $Y_3Fe_5O_{12}$ (YIG), and T_N and $T_{N,YIG}$ are the Neél temperature for $RE_3Fe_5O_{12}$ and YIG, respectively. Here, K_u is given by the sum of the cubic anisotropy constant K_c, growth-induced anisotropy constant K_g, and stress-induced anisotropy constant K_s. Among them, the term of K_s (ref. 19) is the major contribution to the total anisotropy for PLD-grown films:

$$K_u = K_c + K_g + K_s, \tag{6}$$

$$K_u \sim K_s = -\frac{3}{2}\lambda_{111}\sigma_{\parallel}. \tag{7}$$

The calculated relation of W versus t is shown in Fig. 4 using all the known parameters without any fitting parameters; the result shows a fairly good agreement with the experimental data. Small deviation for thicker films may be due to the reduction of the effective $\sigma_{\parallel}$ as mentioned previously. As shown in eqs. (3)–(7), W decreases with decreasing effective $\sigma_{\parallel}$.

In conclusion, we selected $Tm_3Fe_5O_{12}$ as the most plausible compound to realize the perpendicular magnetization in a form of thin film. The films with thicknesses from 46 to 350 nm were prepared to have a coherently strained structure on (111) GGG substrates. The films appeared to have a magnetic hysteresis loop with the perpendicular easy axis, as designed. The magnetic domain structure with a typical maze pattern was observed and the domain size scales with the film thickness in accordance with the scaling law of $W \propto \sqrt{t}$.

Acknowledgment This research was supported by the Japan Society for the Promotion of Science (JSPS) through the "Funding Program for World-Leading Innovative R&D on Science and Technology (FIRST Program)", initiated by the Council for Science and Technology Policy (CSTP). A part of this work was conducted in the Research Hub for Advanced Nano Characterization, The University of Tokyo, supported by the Ministry of Education, Culture, Sports, Science and Technology, Japan (MEXT).

1) A. Paoletti: *Physics of Magnetic Garnets* (North-Holland, Amsterdam, 1978).
2) A. H. Eshenfelder: *Magnetic Bubble Technology* (Springer, New York, 1981).
3) P. Paroli: Thin Solid Films **114** (1984) 187.
4) S. A. Manuilov *et al.*: J. Appl. Phys. **105** (2009) 033917.
5) Y. Krockenberger *et al.*: Phys. Rev. B **83** (2011) 214414.
6) A. S. Logginov *et al.*: Appl. Phys. Lett. **93** (2008) 182510.
7) D. M. Heinz *et al.*: J. Appl. Phys. **42** (1971) 1243.
8) A. Rosencwaig and W. J. Tabor: J. Appl. Phys. **42** (1971) 1643.
9) H. Buhay *et al.*: IEEE Trans. Magn. **31** (1995) 3832.
10) S. Kahl *et al.*: MRS Proc. **720** (2002) H6.7.
11) Y. Krockenberger *et al.*: J. Appl. Phys. **106** (2009) 123911.
12) P. C. Dorsey *et al.*: J. Appl. Phys. **74** (1993) 1242.
13) E. Anastassakis: J. Appl. Phys. **68** (1990) 4561.
14) E. Popova *et al.*: J. Appl. Phys. **90** (2001) 1422.
15) H. Yamahara *et al.*: J. Magn. Magn. Mater. **323** (2011) 3143.
16) P. J. A. van Schendel *et al.*: J. Appl. Phys. **88** (2000) 435.
17) H. J. Mamin *et al.*: Appl. Phys. Lett. **55** (1989) 318.
18) J. C. Slonczewski *et al.*: Appl. Phys. Lett. **24** (1974) 396.
19) E. A. Giess *et al.*: Mater. Res. Bull. **6** (1971) 317.